Advanced Ceramics Progress: Vol. 9, No. 2, (Spring 2023) 16-23

Materials and Energy Research Center
MERC

Contents lists available at ACERP

Advanced Ceramics Progress

Journal Homepage: www.acerp.ir

Original Research Article

The Effect of Temperature and Al as an Additive on the Synthesis, Structure, Densification, and Conductivity of Garnet-Type $Li_7La_3Zr_2O_{12}$

Leila Rezazadeh [a], Susan Hasheminia [a], Zahra Khakpour [b, *]

[a] *Assistant Professor, Department of Mechanic, Marand Branch, Islamic Azad University, Marand, Iran*
[b] *Assistant Professor, Department of Ceramic, Materials and Energy Research Center, Karaj, Iran*

* Corresponding Author Email: z.khakpour@merc.ac.ir (Z. Khakpour)

URL: https://www.acerp.ir/article_172226.html

ARTICLE INFO

Article History:

Received 26 February 2023
Received in revised form 21 May 2023
Accepted 06 June 2023

Keywords:

Li Solid State Electrolyte
Synthesis
Densification
Ionic Conductivity

ABSTRACT

Garnet-type $Li_7La_3Zr_2O_{12}$ (LLZO) solid-state electrolytes are promising candidates for application in next-generation solid-state batteries. Of note, the most controversial issue is to stabilize the cubic phase structure (c-LLZO) with high density after the sinter process to reach high ionic conductivity with the desired strength. Considering this issue, the current study aims to investigate the synthesis and sintering of LLZO with Al substituted and without any additive. The LLZO ceramic was synthesized through conventional solid-state reaction. The effect of heating temperature on the synthesis of the cubic structure was studied using X-Ray Diffraction (XRD). The ionic conductivity of the samples was examined by AC Impedance Spectroscopy. The obtained results indicated that Al doping led to the cubic phase stabilization and that it had a positive effect on the sintering regime so that the sample with Al dopant was densified at the lower temperature of 1140 °C. The total ion conductivity of Al-LLZO is 0.1 $mScm^{-1}$ which is comparable to the values of high temperature-sintered samples.

https://doi.org/10.30501/acp.2023.387377.1119

1. INTRODUCTION

Nowadays, energy crisis is one of the most critical challenges facing most countries. In recent decades, the significant reduction in fossil fuel reserves as well as considerable increase in the environmental pollution caused by fossil fuels consumption have forced governments and industries to find solutions to these problems and achieve superior technology in the field of energy production. Since exploitation of non-conventional energy sources such as wind, solar or nuclear sources is bound to some limitations, the focus is more on the use of batteries and fuel cells to store and produce as much energy as possible [1,2]. Among different types of commercial batteries such as lead, nickel-cadmium, nickel-hydrogen, and lithium batteries, lithium batteries enjoy the energy density of about ten times higher than that of lead and nickel-cadmium batteries in theory. In addition, from an environmental point of view, the presence of toxic elements such as cadmium and lead in these batteries is considered a severe problem such as the expansion of the market for nickel-hydrogen batteries [3]. However, the energy density of these batteries is theoretically still about one-fifth of that of the rechargeable lithium batteries. Lithium batteries have the highest electric driving force (emf)

Please cite this article as: Rezazadeh, L., Hasheminia, S., Khakpour, Z., "The Effect of Temperature and Al as an Additive on the Synthesis, Structure, Densification, and Conductivity of Garnet-type $Li_7La_3Zr_2O_{12}$", ***Advanced Ceramics Progress***, Vol. 9, No. 2, (2023), 16-23. https://doi.org/10.30501/acp.2023.387377.1119

among the other types of batteries. Lithium batteries are used in energy storage and other various applications, including energy consumers and energy transmission and production on a very high scale [2,3]. Currently, Lithium hexa-fluoro phosphate ($LiPF_6$) is practically the only conducting salt used in commercial lithium-ion batteries. However, this type of electrolyte has some major problems and limitations including the leakage of organic electrolytes, freezing at lower temperatures of application environments, and burning at higher temperatures [4,5]. A flexible electrolyte without any leakage is required, especially for energy devices, to enhance the safety levels. To enhance the safety of the LIBs, extended research studies were and still are being conducted to substitute a suitable solid electrolyte (either polymer, or ceramic) with comparable ionic conductivity. However, these polymer and ceramic electrolyte systems have quite low ionic conductivity at the ambient temperature. In ceramic materials, various types of solid-state electrolytes have been investigated, mainly glass or glass ceramics consisting of oxides, sulfides or a mixture of both. Unfortunately, they have either high ionic conductivity or good chemical stability rather than both [5-8]. One of the most recently studied compounds is garnet-type $Li_7La_3Zr_2O_{12}$ (LLZO) that was first examined by Thangadurai et al. [9]. Among the most important reasons behind the increasing attention to LLZO in this field are its wide electrochemical stability window, high ionic conductivity at room temperature, and non-flammability. In addition, compared to other solid electrolytes such as sulfide-based solid electrolytes, lithium-garnet enjoys more excellent chemical thermodynamic stability and particularly, its greater stability against lithium metal is essential [3,6].

The garnet-type LLZO is generally stabilized in a two-phase structure namely the cubic (space group $Ia\bar{3}d$), which is necessary to achieve high ionic conductivity, and tetragonal structure (space group $I4_1/acd$), which is thermodynamically more stable at room temperature. On the contrary, ionic conductivity is two to three orders of magnitude lower than usual [8,10]. The main challenge in the synthesis of LLZO is to reach the ideal cubic conductor phase, which is unpractical in every study with the usual sinter of LLZO bodies. However, Murugan et al. [11] obtained a dense cubic phase with high conductivity. Of note, the results obtained from other groups who followed Murugan's method for synthesis and sintering revealed that the final product contained much more stable tetragonal mainly because the tetragonal phase was thermodynamically more stable and was easily obtained through the usual solid-state reaction sintering method in the temperature range of 950-980 °C [12,13]. Researches remark that to stabilize the preferred cubic phase, it is necessary to use higher temperatures while higher temperatures facilitate and speed up the release and loss of lithium from the electrolyte. Consequently, engineering sintering temperature and storage time, controlling the lithium release reduction, and reaching the cubic phase with the density above 90 % will still remain the essential challenges in the field of LLZO solid electrolyte. Consequently, many researchers in this field have focused on stabilizing the cubic phase. In this regard, many studies on stabilizing the cubic structure of LLZO put their main focus on the dopants such as Al^{3+}, Ga^{3+}, Fe^{3+} substitute for Li^+ sites [6,11,14-18] and Ta^{5+} and Nb^{5+} substitute for Zr^{4+} sites [19,20] to create vacancies in the structure. To lower the sintering temperature, synthesis through a sol-gel process [21] based on the rapid sintering method [22], field-assisted sintering technique [23], and expensive methods such as hot-press or spark plasma sintering methods [24,25] have been investigated. However, using Al, Ga, and Ta as a sintering aid was reported to be effective in increasing the density of the sintered samples [16,17].

In this research, the LLZO electrolyte was synthesized based on a facile solid-state method. In addition, the composition of raw materials was modified, and the synthesis conditions (i.e., temperature, time and atmosphere) were optimized. Finally, the electrochemical analysis was done on the electrolytes by carrying out some detailed tests, evaluating the effects of the composition, grain, and grain boundary conductivity, and determining the best sample for battery construction.

2. MATERIALS AND METHODS

LLZO powder was synthesized through the solid-state method using stoichiometric amounts of Li_2CO_3, La_2O_3 (preheated at 900 °C for 10 h), ZrO_2, and Al_2O_3. An excessive amount of 10 wt. % Li_2CO_3 was then mixed to compensate for the lithium evaporation during the sintering process. The raw materials were mixed through a planetary mill with zirconia balls for six hours in isopropanol under an air atmosphere and then dried at 100 °C. The obtained powder was heated in a furnace in a zirconia crucible (for the sample without Al dopant) and alumina crucible with a lid to prevent lithium loss during heat treatment at 900-1100 ºC for 10 h. In the following step, the mixed powder was reground and pressed into pellets with 16.3 mm diameter at 300 MPa, followed by sintering in the temperature range of 1100-1260 °C for 8 h. The pellets were placed in a small crucible surrounded by layers of mother sacrificial powder to suppress the potential volatilization of Li_2O during the preparation.

The phase compositions of the as-synthesized LLZO powders and sintered pellets were studied by X-ray diffractometry (Philips) using Cu Kα radiation (λ = 1.5417 Å) as the X-ray source in a 2θ range of 10-80 with the step size of 0.02° and step time of 2 s. The relative densities of the obtained ceramic pellets were geometrically estimated and compared to the theoretical density of LLZO. The theoretical density of samples was

calculated from the lattice parameters determined by X-Ray Diffraction (XRD). For the ionic conductivity measurement, gold electrodes were applied to both sides of the sintered bodies by removing the surface layer using a coating of Au paste, drying, and heat treatment at 200 °C for 20 min. The samples were then loaded into a spring-loaded Swagelok cell with stainless steel electrodes. The ionic conductivity tests were carried out in the temperature range of 298-393 K and frequency range of 0.1-2×10^6 Hz. The samples were first heated up and then cooled down to room temperature to do conductivity measurement so as to eliminate any effect of moisture on conductivity. The complex impedance spectra were analyzed using commercially available Z-View software.

3. RESULTS AND DISCUSSION

Figure 1 demonstrates the XRD patterns of the synthesized LLZO powder without Al dopant heated at 950 °C for 10 h and LLZO pellet sintered at 1250 ºC for 8 h. For the sintered sample, the XRD pattern was taken from the crushed pellet. According to the XRD results, the cubic LLZO phase was mainly synthesized at this temperature because it was well matched with the standard pattern known as the cubic garnet phase (PDF# 045-0109). The pyrochlore phase $La_2Zr_2O_7$, however, was regarded as the majority phase of the synthesized powder at 950 °C, indicating that the interaction between Li_2CO_3 and pyrochlore phase $La_2Zr_2O_7$ which leads to the synthesis of LLZO is not yet complete at this temperature. There is also a possibility that a proportion of the LLZO phase is the tetragonal phase that cannot be detected in the XRD measurements.

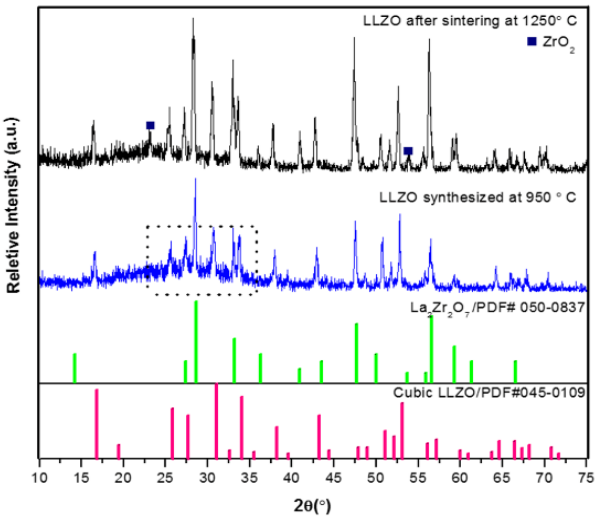

Figure 1. XRD patterns for pure LLZO powder after synthesized at 950 °C for 10 h and pellet after sintered at 1250 °C

Based on some earlier research results [21,26-28], pyrochlore phase $La_2Zr_2O_7$ is the first phase formed (~ 690 °C) during the synthesis process of LLZO. The following phenomenon is the melting of Li_2CO_3 in the temperature range of 700-750 °C [26]. The carbonate melt can react with other phases ($La_2Zr_2O_7$, ZrO_2, La_2O_3) which typically results in the LLZO formation in the temperature range of 750-800 °C when the melted Li_2CO_3 reacts with $La_2Zr_2O_7$ and La_2O_3 according to following equation:

$$7\,Li_2CO_3 + La_2O_3 + 2\,La_2Zr_2O_7 = 2\,Li_7La_3Zr_2O_{12} + 7CO_2 \quad (1)$$

Since the LLZO formation is completed by the melting and reaction of amorphous Li_2CO_3, opting the optimal temperature and reasonable time of the synthesis process is vital. According to the research reports [26], the rate of Li_2CO_3 decomposition is a crucial parameter that determines the LLZO synthesis reaction. The XRD pattern of the synthesized LLZO powder in Figure 1 also illustrates a broad feature, i.e., an amorphous halo, from about 25 to 40 degrees marked by dotted rectangular, confirming that the powder is semi-crystalline or it has an amorphous phase. Consequently, the reaction between the melted Li_2CO_3 and pyrochlore phase has not been yet accomplished at the selected temperature and time. Several studies reported the presence of a secondary $La_2Zr_2O_7$ phase. For instance, Liu et al. [28] showed that the $La_2Zr_2O_7$ phase appeared as a second phase in all the synthesized samples; however, it was removed after the sintering process. Figure 1 illustrates the XRD pattern of the sintered sample at 1250 °C for 8 h, showing more substantial peaks belonging to the LLZO phase than the synthesized powder while a considerable amount of pyrochlore phase is still present. In addition, a small amount of ZrO_2 can be detected. In a study by J. Kosir et al. [21], increasing the temperature led to the decomposition of the LLZO due to the faster Li outgassing that facilitated more formation of $La_2Zr_2O_7$ phase. Consequently, sintering at the high temperature of 1250 °C promoted the formation of off-stoichiometric LLZO compounds and impurities. Figure 2 demonstrates the XRD pattern of the synthesized pure LLZO and Al-doped one at 1100 °C for 10 h. For better comparison and conclusion of the synthesis of Al-doped LLZO, two batches of the weighted stoichiometry of the precursors were prepared to heat up at 950 °C for 8 h and at 1100 °C for 8 h. Upon increasing the temperature, the peaks belonging to C-LLZO get sharper; however, a plenty amount of the unwanted pyrochlore phase is still present and did not disappear. There is also a deviation from the base line in the same range of the XRD as there is in the XRD pattern of pure LLZO at 950 °C (marked by the dotted line in Figure 2).

In this regard, it can be concluded that even by increasing the synthesis temperature up to 1100 °C, the reaction between the melted Li_2CO_3 and pyrochlore phase will not be complete yet. Figure 2 demonstrates the XRD pattern of the $Li_{6.85}Al_{0.15}La_3Zr_2O_{12}$ sample after heating at 950 °C and 1100 °C.

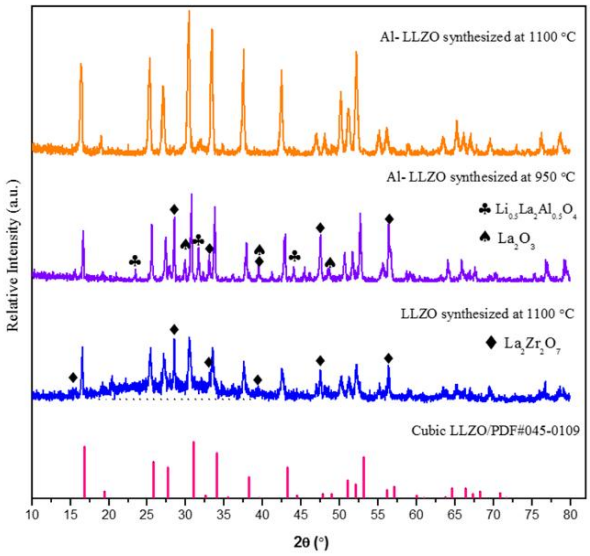

Figure 2. XRD patterns of pure LLZO and Al-LLZO powder synthesized at 950 °C and 1100 °C for 10 h

Accordingly, all the diffraction peaks of the sample heated at 1100 °C can be assigned to the cubic garnet structure. Of note, the final reaction of the sample heated at 950 °C is not complete, and there are still some middle phases present.

As observed, the cubic phase LLZO was synthesized at the lower temperature of 950 °C with other phases of $La_2Zr_2O_7$, $Li_{0.5}La_2Al_{0.5}O_4$, and La_2O_3 still present in lower amounts.

The XRD data of Al-LLZO synthesized at 1100 °C shows very strong and sharp peaks without any shoulder, compared to the pure LLZO (1100 °C), confirming the formation of good crystallinity and high purity of the cubic LLZO.

In order to consider the effect of Al on the sintering and densification of the compounds, pure LLZO and Al-LLZO synthesized at 1100 °C were selected due to the pure LLZO-1100 diffraction peaks assigned to a garnet structure, showing stronger peaks than the same one synthesized at 950 °C. Although the powders were uniaxially pressed and subjected to the same sintering conditions at 1200 °C, eight hours is needed to form dense ceramic pellets, and the densification results were completely different between pure LLZO and Al-LLZO. In the aluminum-doped sample, the specimens under the sintering conditions were bloated and melted in some areas, and 60 % of the theoretical density was the relative density of pure LLZO. As a result, Al-LLZO was sintered at lower temperatures while the pure LLZO was sintered at higher temperatures (i.e., 1230 °C and 1260 °C). Calculation of the geometrical relative densities confirmed that the density increased up to ~ 90 % for the Al-LLZO pellets at the temperatures of 1170 °C and 1140 °C for 8 h. On the contrary, the density of pure LLZO increased up to 68 % with an increase in the sintering temperature up to 1260 °C for 8 h.

The XRD pattern of pure LLZO (Figure 3) is characterized by strong peaks for $La_2Zr_2O_7$ as well as minor characteristic peaks indexed to the LLZO phase.

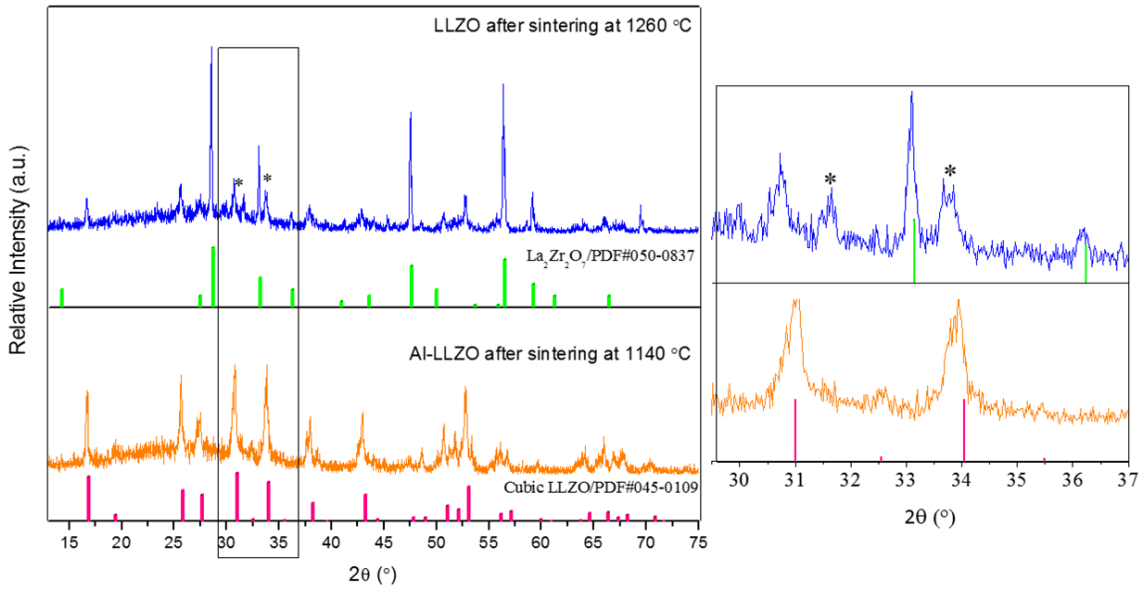

Figure 3. XRD patterns of pure LLZO and Al-LLZO powder synthesized at 950 °C and 1100 °C for 10 h

Compared to the synthesized LLZO powder before sintering (Figure 2), the pure LLZO sample is characterized by a reduction in the peak intensity of the garnet LLZO phase whose diffraction patterns contains both tetragonal and cubic phases, as demonstrated in the magnified view, which shows the split peaks compared to the cubic structure materials. The peaks at $2\theta \approx 31$ and $2\theta \approx 34$ marked by stars in Figure 3 can be split into two peaks that are indicative of the presence of t-LLZO [13]. The XRD pattern of Al-LLZO after sintering (Figure 3) is found to be the cubic garnet LLZO structure with no secondary phases found in the diffraction pattern. Of note, the reduction in the peak intensity of the sintered sample, compared to the Al-LLZO sample, before sintering is notable. Figure 4 illustrates the digital images of the prepared ceramic samples according to which, the sintering ability of pure LLZO sample was quite weak and consequently, it could not be densified properly even by increasing the temperature up to 1260 °C. In contrast to the pure LLZO sample, the Al-LLZO pellet has dense appearance with uniform coloration which is consolidated into a dense body (Figure 4c). A comparison between Figure 4b and 4c reveals that the significant increase in the densities of the Al-LLZO and pure LLZO samples confirms the change in their structures as well as characteristics. While all pure samples sintered between 1200-1260 °C did not densify to reach acceptable pellet densities of over 70 % and remained in a powdered state after sintering (cracked during handling), the Al-LLZO samples were densified at the reduced temperature of 1140 °C with the density of ~ 90 %. A. Paolella et al. [26] investigated the impact of lithium loss during the sintering process of c-LLZO and reported that the pure c-LLZO was metastable and dependent on the sintering time. During the sintering process, the cubic-LLZO becomes tetragonal phase at 1100 °C in the presence of gas flow. As a result, the cubic-LLZO becomes metastable and between c-LLZO and $La_2Zr_2O_7$ impurity before sintering, lithium migration reaction under gas flow occurs. The cubic phase was preserved by intensifying the $La_2Zr_2O_7$ phase, probably due to the lithium loss under no gas flow condition. Therefore, to avoid the pyrochlore $La_2Zr_2O_7$ phase, it is vital to maintain as much lithium as possible. C. Lopez et al. [29] provided a dry O_2 atmosphere to control the sintering conditions and reported the density value of 70 % for the Ga-doped LLZO samples sintered in air at 1085 °C. The density, however, increased as high as 94 % of the theoretical density of the samples sintered in dry O_2. In their research, J. Kosir et al. [21] concluded that the higher amount of excess Li (more than 10 %) along with adding Al as the dopant are the main keys to obtain the densified sample. S. Afyon et al. [30] studied the synthesis of Ga doped Li garnet structure through the modified sol-gel combustion method and showed that lowering the overall powder processing and sintering temperature was both advantageous to avoid Li-losses and an alternative strategy for stabilizing the cubic phase. Another research [18,21] on the Al-doped LLZO confirmed the promoted sintering of samples with the hypothesis that the reaction between Li_2O and Al_2O_3 would form a liquid phase, such as $LiAlO_2$, which enabled a liquid sintering and accelerated densification [28]. Therefore, dopants such as Al can be used to produce the cubic LLZO by lowering the lithium content to create Li vacancies disrupting the long-range lithium order to stabilize cubic structure at room temperature [31]. Moreover, Al_2O_3 assisted in sintering and densification at the lower temperature 1140 °C, rather than above 1200 °C. Here, a lower sintering temperature is more preferable and suitable mainly because it ensures a better morphology and reduces lithium loss during heating.

(a) **(b)** **(c)**

Figure 4. Picture of the LLZO pellets (a) before sintering; (b) LLZO pellet obtained after sintering at 1260 °C for 8 h; (c) Al-LLZO pellet obtained after sintering at 1140 °C for 8 h

Figure 5 presents the results of the AC conductivity measurements (in Nyquist format) for the Al-LLZO sample using Au blocking electrodes in the temperature range of 25-120 °C in the air.

Typically, impedance spectra are composed of three parts based on the frequency range measurement: the high-frequency range corresponds to the bulk resistance, intermediate-frequency flattened semicircle represents the grain-boundary resistance, and low-frequency spike stands for the contribution of the electrode. The Nyquist plots of the Al-LLZO represent only one clear semicircle in the high-frequency region which is attributed to the total conductivity of the Al-LLZO sample and fitted with an equivalent circuit presented in the inset of Figure 5. In this figure, the distance from zero to the intercept of the linear tail with the real axis is the total conductivity. Accordingly, the total ionic conductivity values of the Al-LLZO sintered at 1140 °C were 0.1, 0.28, 0.48, 0.7, and 1.0 mS cm^{-1} at the temperatures of 25 °C, 50 °C, 100 °C, and 120 °C, respectively.

These values are in good agreement with those reported in other studies [26,27,29,32,33]. Of note, in some of these research, operating different atmosphere [29], adding other additives such as Ga, Ta, and using the advanced sintering technics [23] were taken into consideration.

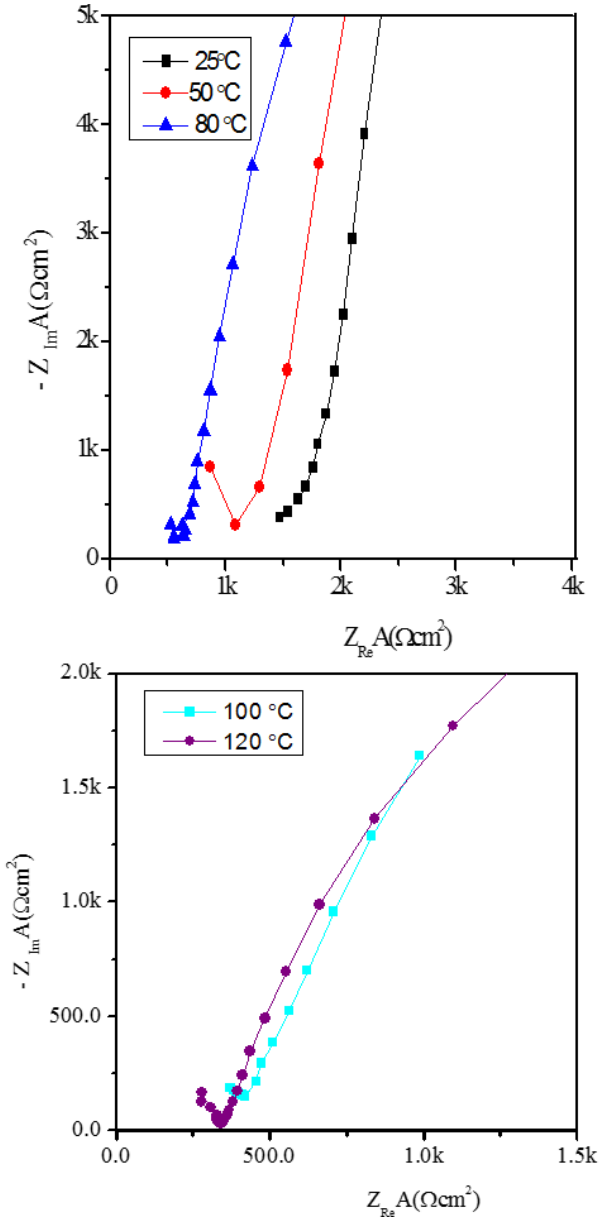

Figure 5. The impedance plots for the Al-LLZO sample sintered at 1140 °C measured at 25, 50, 80, 100, and 120 °C

The Arrhenius equation was used to calculate the activation energy E_a:

$$\sigma T = A \exp(\frac{-E_a}{k_B T}) \quad (2)$$

where σ is the ionic conductivity (Scm^{-1}), A a pre-exponential parameter, k the Boltzmann's constant, and T the absolute temperature. According to Figure 6, the activation energy E_a was measured as 0.27 eV in the temperature range of 25-130 °C, representing high-quality microstructure for moving lithium ions. Since Al-doped sample in this study exhibited the desired sintering behavior and just reached the acceptable density at 1140 °C, the significant role of Al in stabilizing the cubic structure and densification should be proved that would finally lower the activation energy needed for lithium movement in the structure.

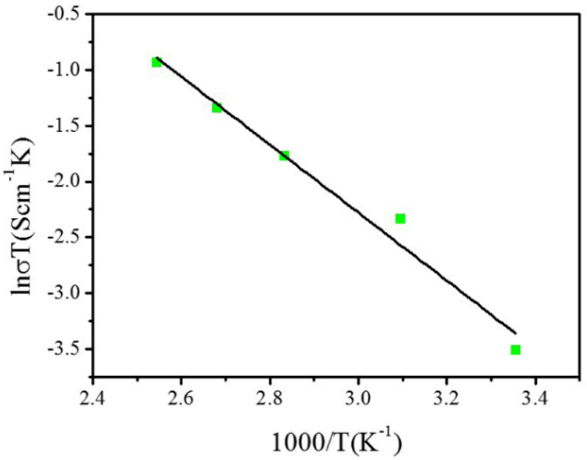

Figure 6. Arrhenius plot of Al-LLZO sample sintered at 1140 °C for 8 h

4. CONCLUSION

In our study, the sintering ability of the synthesized LLZO with Al and without any additive was investigated. The undoped LLZO samples resulted in broken or very fragile strength future after sintering at low or even as high as at 1260 °C temperatures. Lithium loss resulted in low density and transforming to an unwanted phase at high temperature. On the other hand, the Al-doped LLZO resulted in the cubic system, high relative density, and high conductivity. The ionic conductivity of Al-LLZO of 0.1 $mScm^{-1}$ is on the same order of magnitude as most as solid-state electrolytes.

ACKNOWLEDGEMENTS

The authors appreciate use of the ceramic laboratories of materials and energy research center and electrochemical lab facilities.

REFERENCES

1. Fallah Vostakola, M., Amini Horri, B., "Progress in material development for low-temperature solid oxide fuel cells: A review", ***Energies***, Vol. 14, No. 5, (2021), 1280. https://doi.org/10.3390/en14051280
2. Han, X., Gong, Y., Fu, K., He, X., Hitz, G. T., Dai, J., Pearse, A., Liu, B., Wang, H., Rubloff, G., Mo, Y., "Negating interfacial impedance in garnet-based solid-state Li metal batteries", ***Nature***

Materials, Vol. 16, No. 5, (2017), 572-579. https://doi.org/10.1038/nmat4821
3. Tarascon, J. M., Armand, M., "Issues and challenges facing rechargeable lithium batteries", ***Materials for Sustainable Energy***, Vol. 7, (2010), 171-179. https://doi.org/10.1142/9789814317665_0024
4. Zheng, F., Kotobuki, M., Song, S., Lai, M. O., Lu, L., "Review on solid electrolytes for all-solid-state lithium-ion batteries", ***Journal of Power Sources***, Vol. 389, (2018), 198-213. https://doi.org/10.1016/j.jpowsour.2018.04.022
5. Zhu, Y., Gonzalez-Rosillo, J. C., Balaish, M., Hood, Z. D., Kim, K. J., Rupp, J. L., "Lithium-film ceramics for solid-state lithionic devices", ***Nature Reviews Materials***, Vol. 6, No. 4, (2021), 313-331. https://doi.org/10.1038/s41578-020-00261-0
6. Kim, A., Woo, S., Kang, M., Park, H., Kang, B., "Research progresses of garnet-type solid electrolytes for developing all-solid-state Li batteries", ***Frontiers in Chemistry***, Vol. 8, (2020), 468. https://doi.org/10.3389/fchem.2020.00468
7. Afyon, S., Kravchyk, K. V., Wang, S., van den Broek, J., Hänsel, C., Kovalenko, M. V., Rupp, J. L., "Building better all-solid-state batteries with Li-garnet solid electrolytes and metalloid anodes", ***Journal of Materials Chemistry A***, Vol. 7, No. 37, (2019), 21299-21308. https://doi.org/10.1039/c9ta04999a
8. Thangadurai, V., Narayanan, S., Pinzaru, D., "Garnet-type solid-state fast Li ion conductors for Li batteries: critical review", ***Chemical Society Reviews***, Vol. 43, No. 13, (2014), 4714-4727. https://doi.org/10.1039/c4cs00020j
9. Thangadurai, V., Weppner, W., "Recent progress in solid oxide and lithium ion conducting electrolytes research", ***Ionics***, Vol. 12, (2006), 81-92. https://doi.org/10.1007/s11581-006-0013-7
10. Ren, Y., Chen, K., Chen, R., Liu, T., Zhang, Y., Nan, C. W., "Oxide electrolytes for lithium batteries", ***Journal of the American Ceramic Society***, Vol. 98, No. 12, (2015), 3603-3623. https://doi.org/10.1111/jace.13844
11. Murugan, R., Thangadurai, V., Weppner, W., "Fast lithium ion conduction in garnet-type $Li_7La_3Zr_2O_{12}$", ***Angewandte Chemie International Edition***, Vol. 46, No. 41, (2007), 7778-7781. https://doi.org/10.1002/anie.200701144
12. Awaka, J., Kijima, N., Hayakawa, H., Akimoto, J., Synthesis and structure analysis of tetragonal $Li_7La_3Zr_2O_{12}$ with the garnet-related type structure", ***Journal of Solid State Chemistry***, Vol. 182, No. 8, (2009), 2046-2052. https://doi.org/10.1016/j.jssc.2009.05.020
13. Logéat, A., Köhler, T., Eisele, U., Stiaszny, B., Harzer, A., Tovar, M., Senyshyn, A., Ehrenberg, H., Kozinsky, B., "From order to disorder: The structure of lithium-conducting garnets $Li_{7-x}La_3Ta_xZr_{2-x}O_{12}$ (x = 0–2), ***Solid State Ionics***, Vol. 206, (2012), 33-38. https://doi.org/10.1016/j.ssi.2011.10.023
14. Rettenwander, D., Wagner, R., Reyer, A., Bonta, M., Cheng, L., Doeff, M. M., Limbeck, A., Wilkening, M., Amthauer, G., "Interface instability of Fe-stabilized $Li_7La_3Zr_2O_{12}$ versus Li metal", ***The Journal of Physical Chemistry C***, Vol. 122, No. 7, (2018), 3780-3785. https://doi.org/10.1021/acs.jpcc.7b12387
15. Zhuang, L., Huang, X., Lu, Y., Tang, J., Zhou, Y., Ao, X., Yang, Y., Tian, B., "Phase transformation and grain-boundary segregation in Al-Doped $Li_7La_3Zr_2O_{12}$ ceramics", ***Ceramics International***, Vol. 47, No. 16, (2021), 22768-22775. https://doi.org/10.1016/j.ceramint.2021.04.295
16. Matsuda, Y., Sakaida, A., Sugimoto, K., Mori, D., Takeda, Y., Yamamoto, O., Imanishi, N., "Sintering behavior and electrochemical properties of garnet-like lithium conductor $Li_{6.25}M_{0.25}La_3Zr_2O_{12}$ (M: Al^{3+} and Ga^{3+})", ***Solid State Ionics***, Vol. 311, (2017), 69-74. https://doi.org/10.1016/j.ssi.2017.09.014
17. Chen, C., Sun, Y., He, L., Kotobuki, M., Hanc, E., Chen, Y., Zeng, K., Lu, L., "Microstructural and electrochemical properties of Al- and Ga-doped $Li_7La_3Zr_2O_{12}$ garnet solid electrolytes", ***ACS Applied Energy Materials***, Vol. 3, No. 5, (2020), 4708-4719. https://doi.org/10.1021/acsaem.0c00347
18. Xue, W., Yang, Y., Yang, Q., Liu, Y., Wang, L., Chen, C., Cheng, R., "The effect of sintering process on lithium ionic conductivity of $Li_{6.4}Al_{0.2}La_3Zr_2O_{12}$ garnet produced by solid-state synthesis", ***RSC Advances***, Vol. 8, No. 24, (2018), 13083-13088. https://doi.org/10.1039/C8RA01329B
19. Wang, R., Liu, F., Duan, J., Ren, Y., Li, M., Cao, J., "Enhanced electrochemical performance of Al-and Nb-codoped LLZO ceramic powder and its composite solid electrolyte", ***ACS Applied Energy Materials***, Vol. 4, No. 12, (2021), 13912-13921. https://doi.org/10.1021/acsaem.1c02644
20. Yang, L., Tao, X., Huang, X., Zou, C., Yi, L., Chen, X., Zang, Z., Luo, Z., Wang, X., "Efficient mutual-compensating Li-loss strategy toward highly conductive garnet ceramics for Li-metal solid-state batteries", ***ACS Applied Materials & Interfaces***, Vol. 13, No. 47, (2021), 56054-56063. https://doi.org/10.1021/acsami.1c15115
21. Košir, J., Mousavihashemi, S., Wilson, B. P., Rautama, E. L., Kallio, T., "Comparative analysis on the thermal, structural, and electrochemical properties of Al-doped $Li_7La_3Zr_2O_{12}$ solid electrolytes through solid state and sol-gel routes", ***Solid State Ionics***, Vol. 380, (2022), 115943. https://doi.org/10.1016/j.ssi.2022.115943
22. Yang, L., Dai, Q., Liu, L., Shao, D., Luo, K., Jamil, S., Liu, H., Luo, Z., Chang, B., Wang, X., "Rapid sintering method for highly conductive $Li_7La_3Zr_2O_{12}$ ceramic electrolyte", ***Ceramics International***, Vol. 46, No. 8, (2020), 10917-10924. https://doi.org/10.1016/j.ceramint.2020.01.106
23. Zhang, Y., Chen, F., Tu, R., Shen, Q., Zhang, L., "Field assisted sintering of dense Al-substituted cubic phase $Li_7La_3Zr_2O_{12}$ solid electrolytes", ***Journal of Power Sources***, Vol. 268, (2014), 960-964. https://doi.org/10.1016/j.jpowsour.2014.03.148
24. Kim, Y., Jo, H., Allen, J. L., Choe, H., Wolfenstine, J., Sakamoto, J., "The effect of relative density on the mechanical properties of hot-pressed cubic $Li_7La_3Zr_2O_{12}$", ***Journal of the American Ceramic Society***, Vol. 99, No. 4, (2016), 1367-1374. https://doi.org/10.1111/jace.14084
25. Baek, S. W., Lee, J. M., Kim, T. Y., Song, M. S., Park, Y., "Garnet related lithium ion conductor processed by spark plasma sintering for all solid state batteries", ***Journal of Power Sources***, Vol. 249, (2014), 197-206. https://doi.org/10.1016/j.jpowsour.2013.10.089
26. Paolella, A., Zhu, W., Bertoni, G., Savoie, S., Feng, Z., Demers, H., Gariepy, V., Girard, G., Rivard, E., Delaporte, N., Guerfi, A., "Discovering the influence of lithium loss on garnet $Li_7La_3Zr_2O_{12}$ electrolyte phase stability", ***ACS Applied Energy Materials***, Vol. 3, No. 4, (2020), 3415-3424. https://doi.org/10.1021/acsaem.9b02401
27. Rangasamy, E., Wolfenstine, J., Sakamoto, J., "The role of Al and Li concentration on the formation of cubic garnet solid electrolyte of nominal composition $Li_7La_3Zr_2O_{12}$", ***Solid State Ionics***, Vol. 206, (2012), 28-32. https://doi.org/10.1016/j.ssi.2011.10.022
28. Liu, K., Ma, J. T., Wang, C.A., "Excess lithium salt functions more than compensating for lithium loss when synthesizing $Li_{6.5}La_3Ta_{0.5}Zr_{1.5}O_{12}$ in alumina crucible", ***Journal of Power Sources***, Vol. 260, (2014), 109-114. https://doi.org/10.1016/j.jpowsour.2014.02.065
29. Bernuy-Lopez, C., Manalastas Jr, W., Lopez del Amo, J. M., Aguadero, A., Aguesse, F., Kilner, J. A., "Atmosphere controlled processing of Ga-substituted garnets for high Li-ion conductivity ceramics", ***Chemistry of Materials***, Vol. 26, No. 12, (2014), 3610-3617. https://doi.org/10.1021/cm5008069
30. Afyon, S., Krumeich, F., Rupp, J. L., "A shortcut to garnet-type fast Li-ion conductors for all-solid state batteries", ***Journal of Materials Chemistry A***, Vol. 3, No. 36, (2015), 18636-18648. https://doi.org/10.1039/c5ta03239c
31. Thompson, T., Wolfenstine, J., Allen, J. L., Johannes, M., Huq, A., David, I. N., Sakamoto, J., "Tetragonal vs. cubic phase stability in Al–free Ta doped $Li_7La_3Zr_2O_{12}$ (LLZO)", ***Journal of Materials Chemistry A***, Vol. 2, No. 33, (2014), 13431-13436. https://doi.org/10.1039/C4TA02099E
32. Dhivya, L., Karthik, K., Ramakumar, S., Murugan, R., "Facile synthesis of high lithium ion conductive cubic phase lithium garnets for electrochemical energy storage devices", ***RSC Advances***, Vol. 5, No. 116, (2015), 96042-96051. https://doi.org/10.1039/c5ra18543b

33. Li, Y., Han, J. T., Wang, C. A., Xie, H., Goodenough, J. B., "Optimizing Li^+ conductivity in a garnet framework", ***Journal of Materials Chemistry***, Vol. 22, No. 30, (2012), 15357-15361. https://doi.org/10.1039/C2JM31413D